PERMAFROST AND PERIGLACIAL PROCESSES
*Permafrost and Periglac. Process.* (2007)
Published online in Wiley InterScience
(www.interscience.wiley.com) DOI: 10.1002/ppp.594

# Application of Ground-Penetrating Radar Imagery for Three-Dimensional Visualisation of Near-Surface Structures in Ice-Rich Permafrost, Barrow, Alaska

*Jeffrey S. Munroe*,[1]* *Jim A. Doolittle*,[2] *Mikhail Z. Kanevskiy*,[3] *Kenneth M. Hinkel*,[4] *Frederick E. Nelson*,[5] *Benjamin M. Jones*,[6] *Yuri Shur*[3] *and John M. Kimble*[7]

[1] Department of Geology, Middlebury College, Middlebury, VT, USA
[2] USDA-NRCS, Newtown Square, PA, USA
[3] Institute of Northern Engineering, University of Alaska, Fairbanks, AK, USA
[4] Department of Geography, University of Cincinnati, Cincinnati, OH, USA
[5] UD Permafrost Group, Department of Geography, University of Delaware, Newark, DE, USA
[6] US Geological Survey Alaska Science Center, Anchorage, AK, USA
[7] USDA-NRCS, Lincoln, NE, USA

## ABSTRACT

Three-dimensional ground-penetrating radar (3D GPR) was used to investigate the subsurface structure of ice-wedge polygons and other features of the frozen active layer and near-surface permafrost near Barrow, Alaska. Surveys were conducted at three sites located on landscapes of different geomorphic age. At each site, sediment cores were collected and characterised to aid interpretation of GPR data. At two sites, 3D GPR was able to delineate subsurface ice-wedge networks with high fidelity. Three-dimensional GPR data also revealed a fundamental difference in ice-wedge morphology between these two sites that is consistent with differences in landscape age. At a third site, the combination of two-dimensional and 3D GPR revealed the location of an active frost boil with ataxitic cryostructure. When supplemented by analysis of soil cores, 3D GPR offers considerable potential for imaging, interpreting and 3D mapping of near-surface soil and ice structures in permafrost environments. 

KEY WORDS: Alaska; ground-penetrating radar; ice-wedge polygons; permafrost

## INTRODUCTION

Ground-penetrating radar (GPR), a geophysical technique designed specifically for shallow subsurface investigations, is particularly suited to the study of frozen ground. As the soil temperature drops below 0°C, the electrical conductivity, dielectric permittivity, and loss tangent decrease, increasing the suitability of most media for application of GPR (Scott *et al*., 1990). Radar penetration depths also increase as soil water freezes, although subsurface variations may become more difficult to resolve as ice content increases and the contrast in electromagnetic properties between frozen soil layers diminishes. Soil horizons affected by cryoturbation can be particularly difficult to distinguish on radar records because of their high ice content, complicated geometry and close spacing.

* Correspondence to: Jeffrey S. Munroe, Department of Geology, Middlebury College, Middlebury, VT 05753, USA.
E-mail: jmunroe@middlebury.edu

Contract/grant sponsor: US National Science Foundation; contract/grant numbers: OPP-0094769; OPP-0095088; OPP-0352958; EPS-0346770; ARC-0454939.
Contract/grant sponsor: Barrow Arctic Science Consortium.
Contract/grant sponsor: Ukpeagvik Inupiat Corporation.

*Received 19 February 2007*
*Revised 29 May 2007*
*Accepted 11 June 2007*

Soil sampling conducted in concert with GPR surveys can compensate for these limitations by providing information about frozen ground characteristics.

Ground-penetrating radar has been used extensively in permafrost terrain, including studies of variations in active-layer thickness (Pilon *et al*., 1985; Doolittle *et al*., 1990, 1992; Moorman *et al*., 2003; Wu *et al*., 2005) and the relative dielectric permittivity of frozen sediments (Arcone and Delaney, 1989). GPR has also been used to identify and map areas of massive ground ice (Kovacs and Morey, 1985; Dallimore and Davis, 1987; Scott *et al*., 1990; Robinson *et al*., 1993), taliks (Arcone *et al*., 1998), and to examine the internal structure of pingos (Kovacs and Morey, 1985; Ross *et al*., 2005; Yoshikawa *et al*., 2006) and palsas (Seguin, 1986; Doolittle *et al*., 1992; Horvath, 1998).

In a GPR study near Barrow, Alaska, Hinkel *et al*. (2001) demonstrated that ice wedges form the most conspicuous subsurface reflections in two-dimensional (2D) radar profiles. The dielectric properties of ice wedges contrast sharply with the surrounding perennially frozen materials and produce identifiable, high-amplitude hyperbolic reflections. Hinkel *et al*. (2001) also demonstrated that the long-term position of the permafrost table can be traced laterally across radar records because of ice-enrichment immediately below the active layer.

Recent developments in data-processing software allow the geometry and structure of subsurface features to be analysed in three dimensions by combining data from multiple, closely spaced radar traverses. Three-dimensional GPR (3D GPR) has been used extensively in archaeological (Conyers and Goodman, 1997; Grasmueck *et al*., 2004; Leucci and Negri, 2006) and infrastructure investigations (Sudarmo *et al*., 1996). It has also been used to characterise sedimentary sequences and the internal structure of sedimentary rocks (Corbeanu *et al*., 2002; Szerbiak *et al*., 2001; Grasmueck *et al*., 2004), karst terrains (Kruse *et al*., 2006), glacial drift (Beres *et al*., 1995; Asprion and Aigner, 1999), faults (Green *et al*., 2003) and dunes (van Dam, 2002). In each of these investigations, the ability of 3D GPR to characterise the structure and geometry of subsurface features was influenced by the soil environment, the number of ground-truth observations and existing knowledge of the study sites.

In recent years, a type of 3D GPR data manipulation known as 'amplitude slice-map analysis' has been used in several investigations (e.g. Conyers and Goodman, 1997; Aspiron and Aigner, 1999; Lehman and Green, 1999). In this procedure, the amplitude difference of reflected radar energy is averaged between adjacent parallel radar traverses within a specific time (i.e. depth) interval (Conyers and Goodman, 1997). The result, a map depicting the distribution of reflected wave amplitude, represents lateral changes in soil properties or the presence of subsurface features.

Although 3D GPR holds considerable potential for studying the 3D geometry of ice-wedge networks, review of the literature suggests it has not been used widely as an interpretive tool in permafrost environments. In this paper we report an application of 3D GPR techniques to ice-rich permafrost on the Arctic Coastal Plain of northern Alaska. Surveys were run at three separate sites to evaluate the suitability of this method for use in ice-rich sediments, and to assess the potential of 3D GPR for enhancing imaging, identification and interpretation of subsurface ice-wedge polygons. Cores of frozen sediment were collected simultaneously at each site to aid interpretation of the 3D GPR data.

## STUDY AREA

Fieldwork was conducted on the Barrow Environmental Observatory (BASC, 2007) at the northern limit of Alaska's Arctic Coastal Plain. Barrow has a cold maritime climate, with a mean annual air temperature (1949–2006) of $-12.2^{\circ}$C and mean annual precipitation of 117 mm (WRCC, 2006). The entire area is underlain by permafrost, with maximum thickness in excess of 400 m (Wahrhaftig, 1965). Active-layer thickness averages 35 cm, but varies from 30 to 90 cm depending on vegetation, snow cover and microtopography (Hinkel and Nelson, 2003).

The Arctic Coastal Plain is comprised of nearly level to very gently rolling terrain dotted by a large number of thaw lakes, many of which are elongated in a north-northwesterly direction (Carson and Hussey, 1962; Hinkel *et al*., 2003, 2005; Frohn *et al*., 2005). These lakes enlarge and deepen through thermal and mechanical erosion, and eventually drain into intersecting streams or lower lake basins. Interpretation of remotely sensed imagery indicates that nearly 75% of the area around Barrow is covered by contemporary thaw lakes or drained thaw-lake basins (Hinkel *et al*., 2003). Ice-wedge polygons commonly develop along the floors of these lakes following drainage (Hopkins, 1949; Britton, 1966; Billings and Peterson, 1980).

Sellmann *et al*. (1975) reported 50 to 75% ice by volume in the upper 2 m of permafrost in the vicinity of Barrow. Ice occurs in pores, and as veins, nets and lenses. Ice wedges locally occupy an additional 10% to 40%. Ice lenses are typically concentrated near the base of the active layer, where conditions favour



DOI: 10.1002/ppp

gradual refreezing of soil water (Brown, 1967; Mackay, 1983). The upper part of the permafrost, known as the transition zone, is oversaturated with ice and often displays well-developed ataxitic (suspended) cryostructure (Shur *et al*., 2005). Near Barrow, the most dynamic part of this zone, known as the transient layer, extends to an average depth of 57 cm, which is several decimetres below the base of the average active layer (Bockheim and Hinkel, 2005).

Three-dimensional GPR surveys were run at three sites, each selected for different objectives (Figure 1). The Arctic System Science (ARCSS)/Circumpolar Active Layer Monitoring (CALM) Grid (AG) site (71.30785° N, 156.59025° W) was established to determine the ability of 3D GPR to distinguish permafrost and active-layer features within fairly homogenous ice-enriched sediments. The AG site is located in an area of high-centre polygons within a thaw-lake basin 50 to 300 years old (Hinkel *et al*., 2003). The site is within the 1-km$^2$ study grid administered under the CALM programme (Brown *et al*., 2000; Hinkel and Nelson, 2003). Well-defined ice-wedge troughs, generally less than 50 cm deep and 75 to 150 cm wide, delineate a network of ∼10-m wide polygons. Well-developed frost boils, ranging from 1 to 2 m in diameter, occupy many of the relatively dry, flat polygon centres (Brown and Johnson, 1965).

The Footprint Lake (FL) site (71.26250° N, 156.64806° W) was established to test the ability of 3D GPR to image ice-wedge networks predicted to exist below a surface obscured by ponded water and aquatic vegetation. The FL site is at the southern end of a thaw lake that was drained artificially around 1950. Thin layers of organic materials and silty lake sediment blanket the basin floor and in summer the site is under 0.5 to >1.5 m of standing water. Scattered

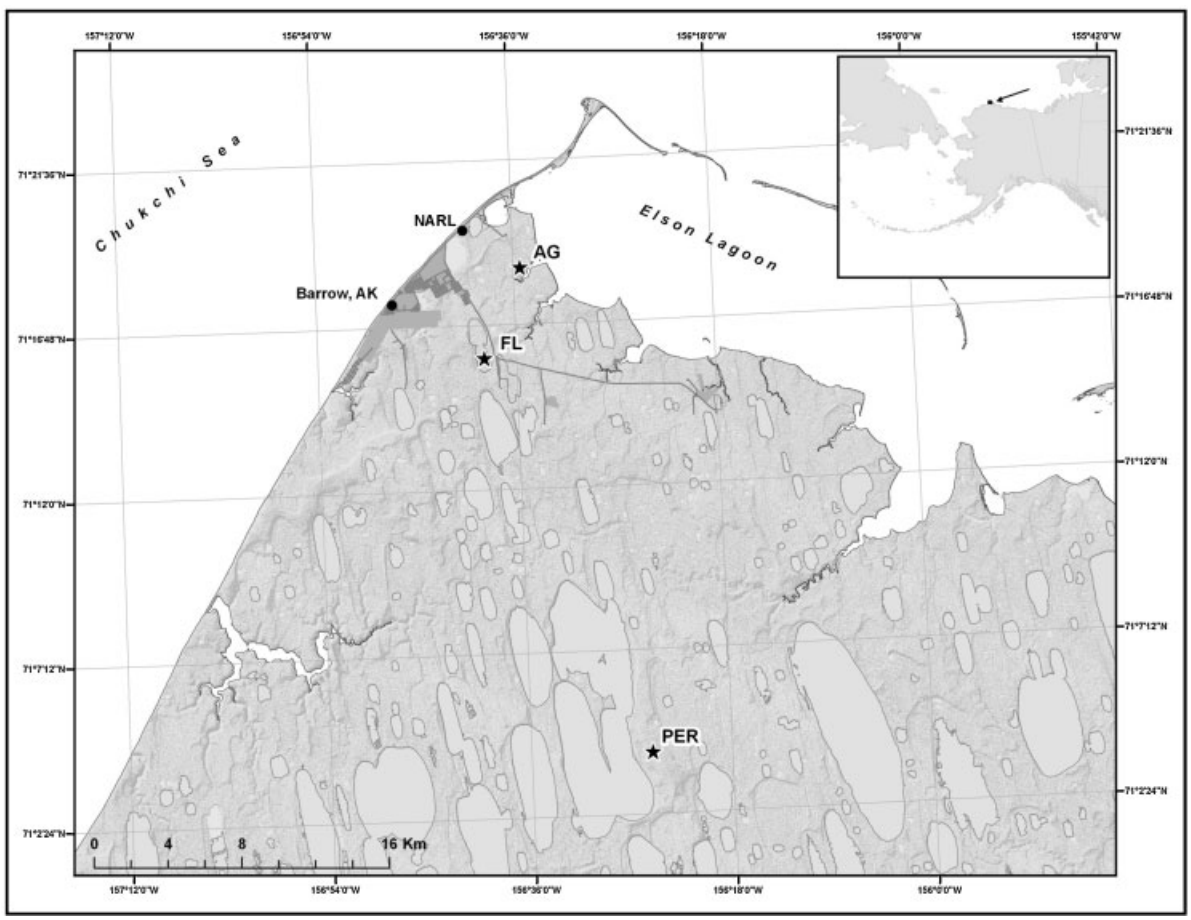


Figure 1 Map showing the location of Barrow, Alaska (inset) and locations of the three study sites (AG, FL and PER). NARL (Naval Arctic Research Laboratory) marks the headquarters of the Barrow Environmental Observatory.



DOI: 10.1002/ppp

ice-cored frost mounds, ranging from 5–20 m across, rise 20–40 cm above the water level (Hinkel *et al*., 1996).

The PER site (71.07331° N, 156.42285° W) is located on the Peterson Erosional Remnant described by Eisner *et al*. (2005). This broad, flat upland is the oldest (9000 BP) and highest (20 m asl) geomorphic surface in the Barrow area. The PER is occupied by high-centred ice-wedge polygons 5 to 10 m in diameter and generally less than 1 m high. Three-dimensional GPR was utilised on the PER to determine how the ice-wedge network beneath this much older landscape surface contrasts with the younger network thought to exist below the FL site.

## METHODOLOGY

Because a thawed active layer with relatively high moisture content is highly attenuating to radar energy, fieldwork was conducted from 18–21 April 2006, when the active layer was completely frozen. During this period the air temperature ranged from −33 to −19°C and the study sites were blanketed by snow ranging in thickness from 0 to 70 cm (mean of ∼30 cm). The general location of each site was selected during the summer of 2005, and approximate locations for the survey grids were marked with stakes and GPS coordinates. For the 3D GPR surveys, a grid was established at each site: 30 × 30 m at the AG and PER sites, and 40 × 40 m at the FL site. Along two parallel axes, survey flags were inserted into the snow at 50-cm intervals and a distance-graduated rope was strung between matching flags on opposite sides of the grid. The antenna was towed by hand at a walking pace along the graduated rope on the snow surface and, as it passed the 100-cm graduations, a mark was impressed on the radar record. Following data collection, the reference line was sequentially displaced 50 cm to the next pair of survey flags to repeat the process. A total of 61 parallel traverses were required for the smaller (30-m) grids and 81 traverses for the larger 40-m grids.

A TerraSIRch Subsurface Interface Radar (SIR) System 3000® with a 400-MHz antenna (manufactured by Geophysical Survey Systems, Inc. (GSSI), Salem, NH), was utilised in the field. On the basis of previous work in the area (Hinkel *et al*., 2001), the 400-MHz antenna was known to provide the best balance between resolution and depth of penetration. Using an SIR-3000 control unit, 48 scans were collected per second, corresponding to ∼50 scans per metre.

Radar records were processed with RADAN for Windows 5.0 (GSSI). Processing included setting the initial pulse to time zero, colour transformation, marker editing, distance normalisation, high-pass horizontal filtration and range gain adjustments. Further processing of all radar records included migration to reduce hyperbolic diffractions and to correct the geometry of inclined soil horizons and stratigraphic layers. For each site, 3D perspective block diagrams, cross sections and time slices were constructed from the radar data using 3D QuickDraw for RADAN Windows NT (GSSI).

For depth calculations, a relative dielectric permittivity (Er) of 5.2 was used, yielding a signal propagation velocity of 0.13 m/ns. These values were determined by previous work in the Barrow area using 2D GPR data verified by soil coring (Hinkel *et al*., 2001). Spatial variability in snow thickness, ice content and soil properties does exist within each survey grid, and this velocity estimation is therefore an approximation. Nonetheless, figures show estimated depth rather than two-way travel time to provide the reader with a more readily interpreted measure.

To provide information about the spatial variability of soil and ground ice conditions in the vicinity of the survey grids, cores were collected from the frozen active layer and upper permafrost using a hydraulic earth drill equipped with a 7.5-cm diameter Snow, Ice and Permafrost Research Establishment (SIPRE) core barrel (Rand and Mellor, 1985). A total of 18 cores, ranging from 80 to 115 cm in length, were obtained. Many of these cores were collected from the vicinity of the GPR grid while the radar data were acquired to assess general soil and ground ice conditions. After review of the unprocessed GPR data in the field, several locations within the grid were targeted for additional coring. In the lab, cores were photographed and sketched, soil horizons were identified and samples were taken by cutting the frozen core with a rock saw. Gravimetric moisture content was calculated from the mass lost after drying for three days at 70°C.

All three sites were revisited during snow-free conditions in August 2006, allowing the context of the GPR grid and coring locations to be further evaluated.

## RESULTS AND INTERPRETATIONS

### ARCSS/CALM Grid Site — AG

Figure 2a shows a representative radar record from this site while Figure 2b illustrates the cryogenic structures and properties of the four soil cores collected there. Sets of sub-parallel reflections visible in the upper part of the profile may represent primary



DOI: 10.1002/ppp

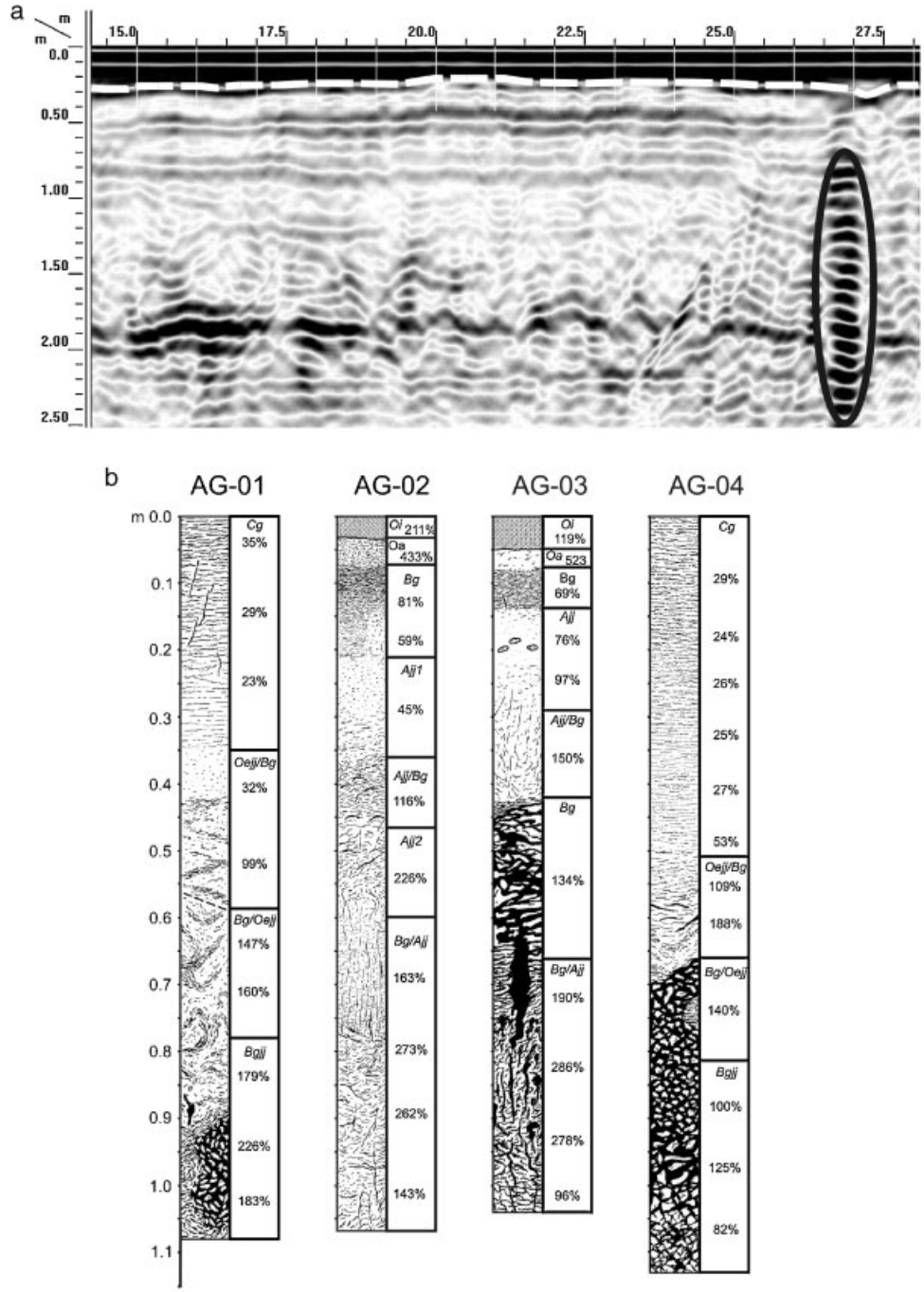


Figure 2 (a) Representative 2D GPR profile and (b) illustrations of cryostructures and soil horizonation in cores from the ARCSS/CALM Grid (AG) site. The horizontal scale on the radar record represents distance in metres; short white vertical lines at the top of record represent equally spaced graduation marks (see text). Vertical depth scale (m) is based on assumed propagation velocity of 0.13 m/ns. A dashed white line was added to highlight the snow/soil interface near a depth of ~0.3 m. The ellipse highlights a high-amplitude reflection with reverberations beneath the 27 m horizontal mark. The values adjacent to the core logs refer to gravimetric soil moisture content in per cent. Soil horizonation follows US Soil Taxonomy (Soil Survey Staff, 2003).



DOI: 10.1002/ppp

stratigraphy in the fine-grained lacustrine sediments of the drained thaw-lake basin. Alternatively, they may represent the permafrost table and related reverberations. The overlapping signals in this part of the record, the differing propagation velocities of radar waves in the frozen substrate and the overlying snow prevent precise characterisation. In the lower part of the record (below ~100 cm) radar reflections are less planar, possibly indicating a relative abundance of segregated ice at this depth.

After evaluation of the radar records in the field, the location of a highly unusual radar signature was identified (highlighted by the ellipse in Figure 2a). Removal of snow from the corresponding location on the survey grid revealed the unvegetated surface of an active frost boil. A core taken (core AG-04, Figure 2b) from the centre of the boil contained abundant thin ice lenses and platy soil structure in the upper 70 cm, and well-developed ataxitic cryofabric from the 70-cm level to the maximum coring depth of 111 cm. The high ice content of this deeper material (approximately four times greater than the unweathered Cg horizon at the surface) is probably responsible for the prominent reflection with reverberations shown on the radar record. Coring in an inactive, vegetated frost boil (AG-01) revealed a similar thin platy structure and abundant thin ice lenses in the Cg material of the upper 30 cm, with extensive cryoturbation and ataxitic structure below 60 cm. In contrast, the two pedons cored between frost boils (AG-02 and AG-03) contained organic horizons over moderately weathered Bg horizons. Both profiles contained cryoturbated horizons at depth, but only one (AG-03) contained ataxitic fabric, indicating a high degree of local variability in cryostructure.

Overall, the 3D GPR records from the AG site accurately captured the microtopography of the land surface and clearly resolved the contrasting soil and cryostructure within the active frost boil (AG-04). However, the 3D GPR instrument array we employed was unable to image the subsurface ice-wedge network, even though a polygonal pattern is obvious at the surface in summer. This result may indicate insufficient contrast between the ice-rich sediment and ice wedges. Alternatively, the ice wedges below this site may be too deep or poorly developed to be imaged from the surface with a 400-Mz antenna. Previous studies (Brown, 1969; Estabrook and Outcalt, 1984) noted that the upper surfaces of some ice wedges are located below the base of the active layer in the Barrow area, demarcating the long-term permafrost table at the base of the transient layer (Shur *et al.*, 2005). Furthermore, given the relative youth of the thaw-lake basin in which site AG is located, which was considered of 'medium' age (50 to 300 yrs) by Hinkel *et al.* (2003), ice wedges that have aggraded into previously unfrozen lake sediment after lake drainage may be thin and difficult to image. The absence of massive ice at depth in the four cores retrieved from this site (to depths of 110 cm) is consistent with this explanation.

## Footprint Lake Site — FL

Results from the 3D GPR survey at the FL site are presented in Figure 3a. Because the image has not been corrected to account for microtopography, the block perspective diagram is shown with a level surface. On the planar Barrow landscape, this simplification does not impact interpretation substantially. In the vertical slices shown in the cutout, the uppermost subsurface reflection represents the snow/organic layer contact (see A in Figure 3a). This interface, though variable in expression, is continuous across the survey area, with a slightly wavy appearance due to the modest (5 to 50 cm) variations in snow depth.

Low- to moderate-amplitude reflections (red and blue) occur in the upper part of the block diagram. These reflections parallel the soil surface in gently sloping layers, possibly delineating ice-rich organic and silty lacustrine sediments accumulated within this thaw-lake basin. Slight convexities along the back wall of the block diagram represent frost mounds. These mounds were not well expressed on the radar records, either because boundaries are more gradational and admixed in these soils, or because abundant frozen water masks these interfaces.

In the lower part of Figure 3a, reflections have higher signal amplitudes and appear more undulating, indicating contrasting material properties over short distances. This overall pattern indicates greater quantities of segregated ice in the deeper sediment. This inference is supported by the presence of gravel at depths of ~1 m in some cores from the site. Furthermore, although the radar data were migrated during processing to remove interference patterns, some diffraction tails persist in the perspective block diagram, indicating the presence of massive ice and inclined strata. It is likely, therefore, that the higher amplitude reflections in the lower part of this diagram represent coarser-textured, ice-rich materials (B in Figure 3a).

The base of the 1.2-m deep cutout reveals linear patterns of moderate- to high-amplitude reflections, with orthogonal junctions interpreted as an ice-wedge network (Figure 3a). High-amplitude reflections and reverberations are apparent where these linear features intersect walls of the block diagram, providing cross



DOI: 10.1002/ppp

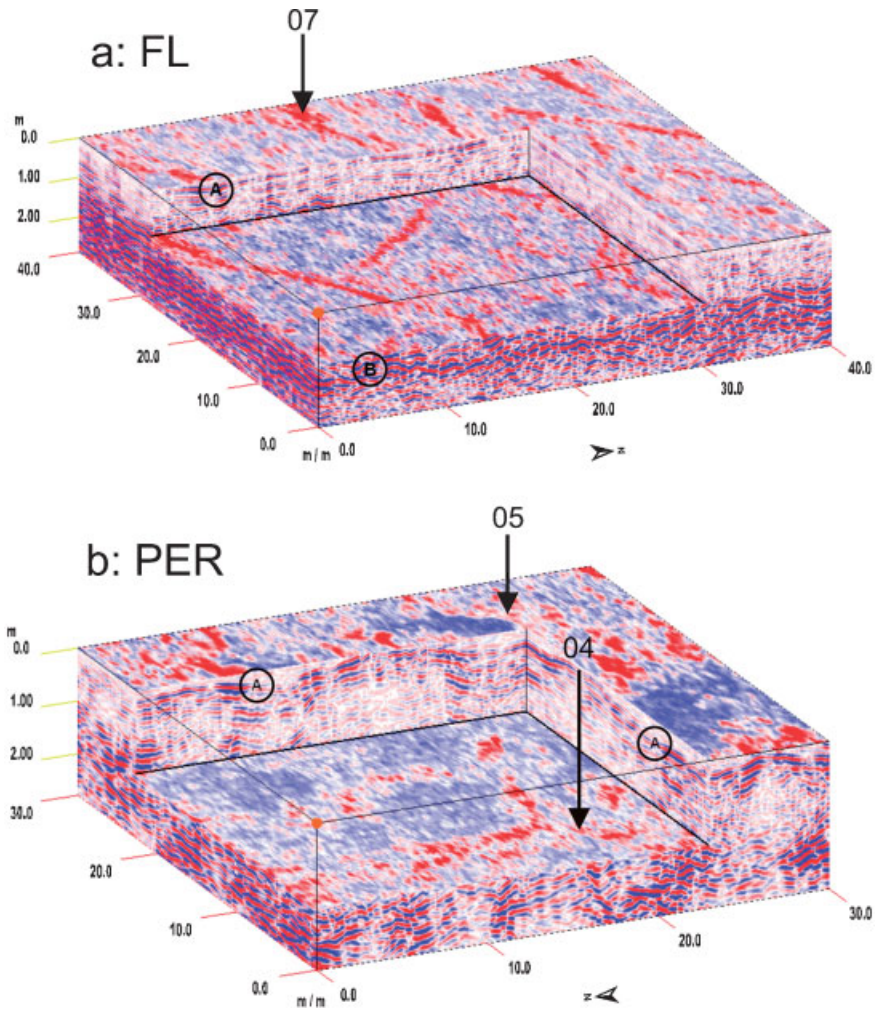


Figure 3 Three-dimensional GPR images from (a) the 40 × 40-m grid at FL and (b) the 30 × 30-m grid at the PER sites. For the FL image, a 30 × 29 × 1.2-m volume has been removed; in the PER image the cut-out is 23 × 23 × 1.6-m. Radar traverses were conducted along the right foreground axis at both sites, producing highly resolved subsurface data. Along the other axis, data were interpolated over the 50 cm between adjacent traverses and the resulting record is less resolved and more generalised. Letter A on the backwall of both cut-outs denotes the contact between the snow and the soil surface. Letter B in Figure 3a highlights notable high-amplitude reflections, interpreted as coarser material with abundant segregated ice. Arrows mark the locations of soil cores retrieved from within the survey grids.

sections through the ice wedges. Many of these features were not obvious on 2D radar records from this site because they did not offer sufficient contrast with surrounding material and were obscured by other reflections. Because most of the site is covered with at least 50 cm of water in summer and the bottom is obscured by aquatic vegetation, there is no obvious evidence of polygonisation at the surface. Application of 3D GPR techniques, therefore, greatly enhances our ability to identify and interpret these features in this setting.

Planimetric views of three time-slice images of the FL site are shown in Figure 4a. Variability in the uppermost slice represents differences in surface microtopography and snow depth. High-amplitude reflections represent slightly higher, convex frost mounds that have minimal snow cover. In the 60-cm slice, subtle variations in signal amplitude and indistinguishable spatial patterns are interpreted to reflect fairly homogenous soil materials. An ice-wedge network is well expressed in the 120-cm slice where the ice wedges have adequate size and sufficient



DOI: 10.1002/ppp

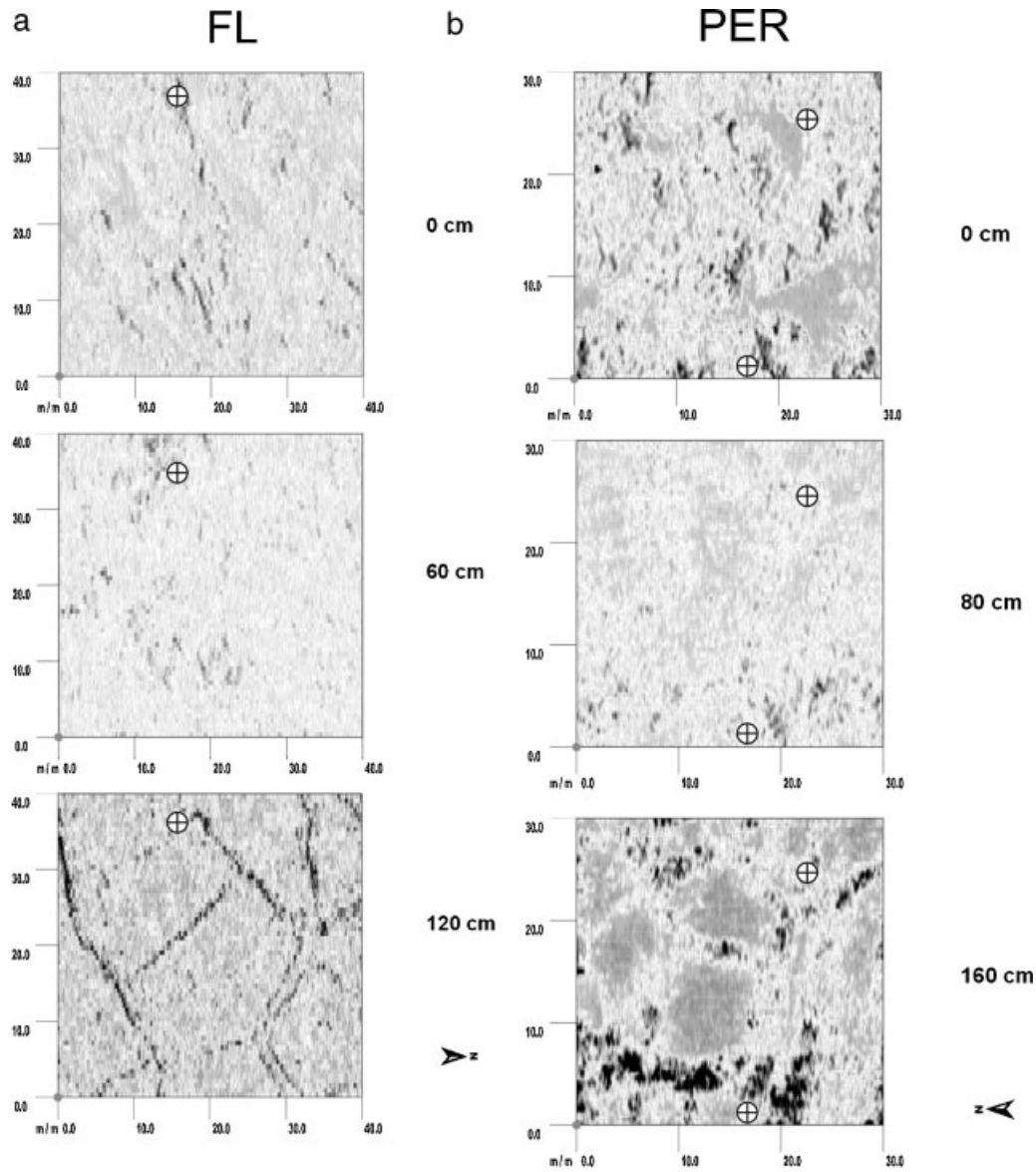


Figure 4 Planimetric time-slice images for the (a) FL and (b) PER sites. The thickness of each slice is 0.19 m. Cross-hairs mark the locations of soil cores retrieved from within the survey grids: PER-04 near bottom centre, PER-05 at upper right. The deepest slice for each site reveals a polygonal network of ice wedges. These features are slender and well defined beneath the recently drained FL, while those beneath the PER are broader and more variable in expression, consistent with the much greater age (∼9000 BP) of this landscape.

contrast in dielectric properties with the bounding permafrost to reveal spatial patterns. The wedges intersect, outlining polygons with a mean diameter of 15 to 20 m. Closely spaced, multiple or bifurcated patterns are also evident, indicating that pairs of ice wedges locally run parallel to one another. Because none of the soil cores from this site (see Figure 5) encountered wedge ice at depths to 110 cm, the 120 cm level must closely constrain the tops of the wedges. The strong reflections outlining wedge geometry are not present in sequentially deeper slices (not shown), despite penetration of the radar pulse to ∼300 cm. We



DOI: 10.1002/ppp

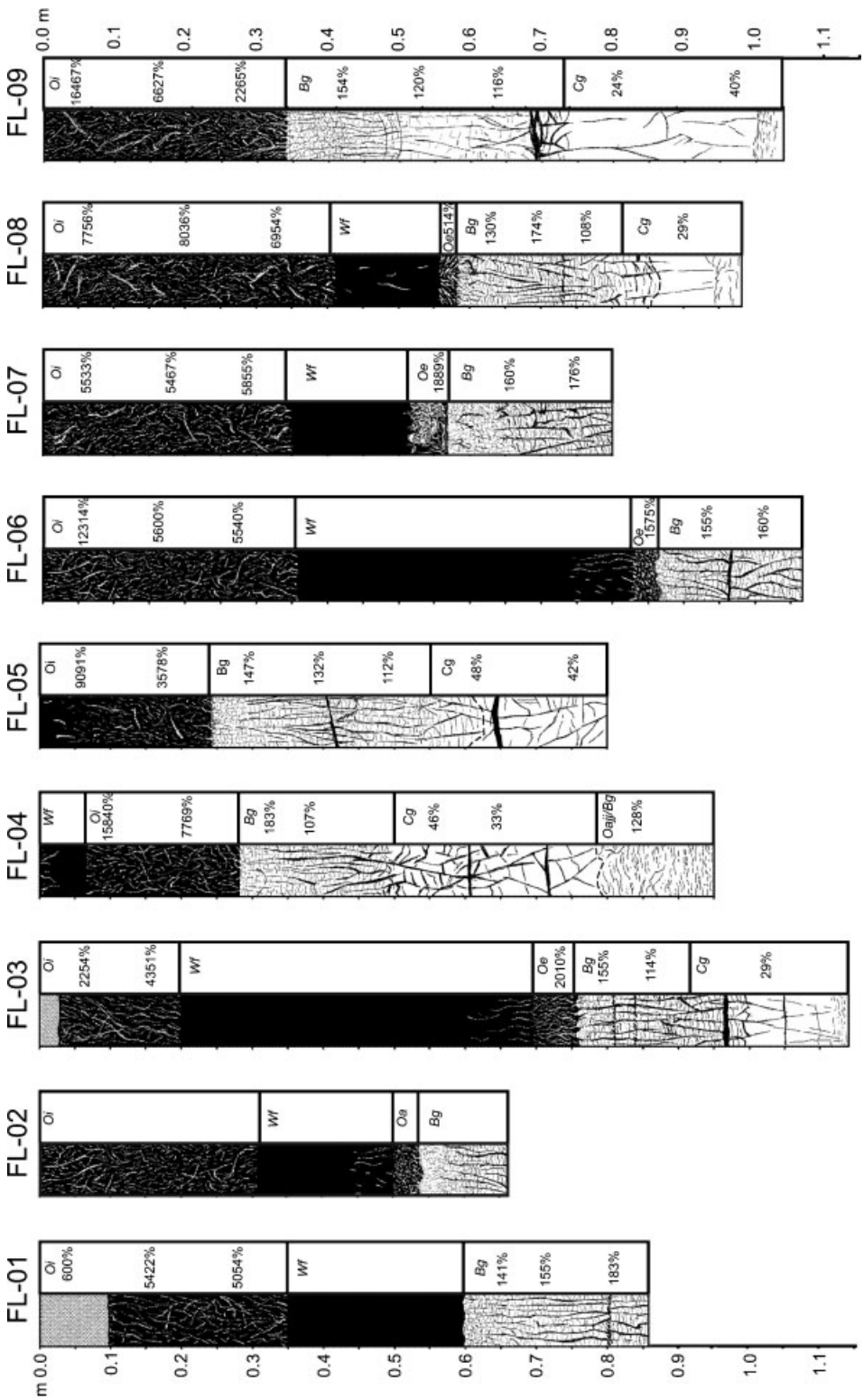


Figure 5 Soil horizonation, cryogenic structure and gravimetric moisture content for nine cores taken from the FL site. Cores FL-01, 02, 03, 06, 07 and 08 were collected from low-lying frost mounds with ice cores (Wf horizons). Deeper cores penetrated gleyed mineral soil (Bg and Cg horizons) representing either lacustrine or marine sediment.



DOI: 10.1002/ppp

interpret this situation to be a consequence of the incipient nature of the ice-wedge network in this recently drained thaw-lake basin.

### Peterson Erosional Remnant Site — PER

Figure 3b shows a perspective view of the 3D GPR sampling grid at the PER site. The surface of the perspective block diagram, which has not been terrain corrected, approximates the snow surface. In the upper part of the cutout's vertical walls the uppermost continuous subsurface reflector (A in Figure 3b) represents the snow/soil contact. This interface is nearly continuous across the survey area, and its wavy appearance reflects the relatively large (2 to 70 cm) differences in snow depth across this site, which is dominated by high-centred ice-wedge polygons. Variations in signal amplitude represent changes in surficial materials, topography, and reflection coefficients (snow with ice, ice-rich organic, or ice-rich mineral soil layers).

Continuous low- to moderate-amplitude reflections in the upper part of the soil exhibit a hummocky expression that mirrors the microtopography of the

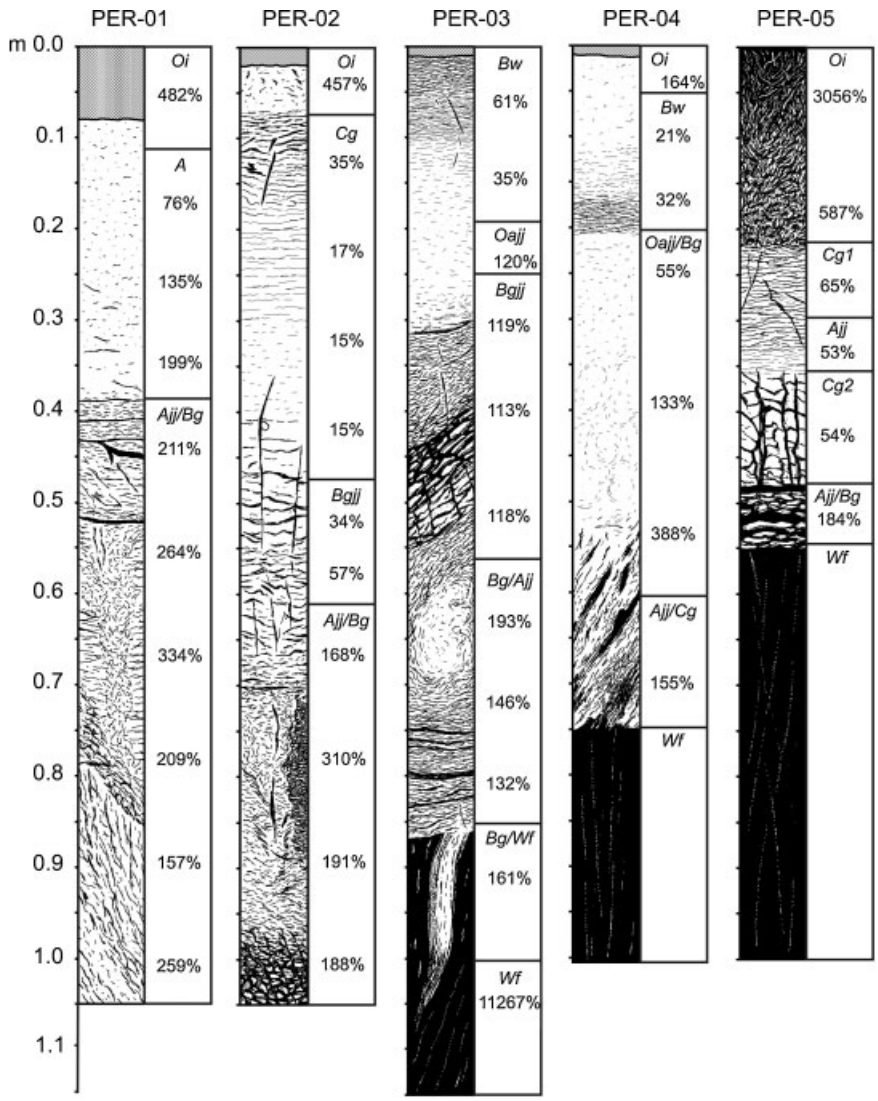


Figure 6 Soil horizonation, cryogenic structure and gravimetric moisture content for five cores taken from the PER site. Three cores (PER-03, 04 and 05) encountered foliated massive ice at depth (Wf) interpreted as wedge ice.



DOI: 10.1002/ppp

high-centred polygons, becoming more convex approaching the surface in polygon centres and more concave beneath ice-wedge troughs. In general, signals are more attenuated beneath the higher portions of polygons, indicating lower ice content.

Reflections are more chaotic in the lower part of Figure 3b, possibly indicating increased abundance of segregated ice. The base of the 1.6-m deep cutout reveals the broad linear patterns of a mature ice-wedge network, identified by linear reflections with varying signal amplitudes that intersect at orthogonal junctions. Similar to the imagery from the FL site (Figure 3a), high-amplitude vertical reflections and reverberated signals are evident where these linear features intersect the walls of the block diagram. However, ice wedges at the PER site are wider and deeper than those at the FL site, with better vertical expression. The ice-wedge network is also more intricate at the PER site, where multiple reflections from wedge tops indicate irregular bounding surfaces with surrounding sediments and possible wedge bifurcations. In the floor of the cutout, the segmented or broken appearance of the ice wedges may be caused by attenuation of the GPR signal from overlying features. The cross section through the ice-wedge polygon cores visible along the back wall of the block diagram (Figure 3b) reveals fairly uniform areas with moderate amplitude reflections.

Planimetric maps of the PER site are shown in Figure 4b. In the surface slice, high-amplitude reflections represent areas that lack or have very minimal snow cover. Compared with the same interface from the FL site (Figure 4a), this slice contains a larger number of high- and moderate- amplitude reflections in a more irregular arrangement, indicating that the microtopography of the PER site is more hummocky than at the FL site. In the 80-cm slice, arcuate bands and broad speckled patterns are interpreted as areas with higher ice contents. As in Figure 4a, the deepest slice reveals an ice-wedge network. Reflection patterns for ice wedges at PER, however, appear broader, more segmented, variable in expression and closely spaced. These characteristics are compatible with a mature stage of ice-wedge development below this relatively old surface.

The inference of large volumes of massive ice in the subsurface at this site is supported by the soil cores, three of which encountered massive foliated ice, interpreted as wedge ice at depths of 55 to 95 cm (Figure 6). Two of these cores (PER-4 and PER-5) were taken from within the GPR grid at the locations of strong reflectors. Eisner *et al*. (2005), who reported massive ice in 90% of soil cores taken from the PER, noted that large amounts of segregated ice are consistent with the relatively great age of the PER, and suggested that some of the site's topographic prominence may be attributable to heave resulting from the ice-segregation process.

## CONCLUSIONS

Three-dimensional GPR data obtained near Barrow, Alaska provide new perspectives on subsurface ice-wedge networks and other features of the frozen active layer and near-surface permafrost. Used in conjunction with data obtained from soil cores, 3D GPR data can identify subtle geocryological phenomena, providing a basis for local surveys based on GPR data. Examples in this study include: (a) active and inactive frost boils with abundant thin ice lenses near the surface; (b) ice-enriched soil with ataxitic cryostructure at depth in a thaw-lake basin believed to have drained within the last 300 years; (c) well-developed ice-wedge networks lacking surface expression because of obscuration by water and vegetation and; (d) contrasts in the 3D structure of ice-wedge networks that are consistent with known age difference between two sites.

Three-dimensional GPR offers great potential for visualising subsurface ice structures, including the subsurface geometry of ice-wedge networks and their variation in 3D. When supplemented with analysis of soil cores, 3D GPR offers considerable potential for imaging, interpreting, and 3D mapping of near-surface soil and ice structures in contemporary permafrost environments. Three-dimensional GPR survey also provides an improved basis for genetic interpretation of relict periglacial features. Information about the 3D geometry of ice-wedge networks in contemporary periglacial environments, rarely obtained prior to this study (see French, 2007, pp. 117–123), provides a quantitative basis for comparison with pseudomorph networks in mid-latitude environments (J. A. Doolittle, unpublished data).

## ACKNOWLEDGEMENTS

This work, a contribution to the CALM programme, was supported by the US National Science Foundation through grants OPP-0094769 to KMH, OPP-0095088 and OPP-0352958 to FEN, and EPS-0346770 and ARC-0454939 to MZK and YLS. Any opinions, findings, conclusions, or recommendations expressed in this material are those of the authors and do not necessarily reflect the views of the National Science Foundation. Mention of any product does not consti-



DOI: 10.1002/ppp

tute endorsement. Thoughtful reviews by Chris Hugenholtz and Kurt Roth are appreciated. The authors appreciate support from the Barrow Arctic Science Consortium and the Ukpeagvik Inupiat Corporation.

## REFERENCES

Arcone SA, Delaney AJ. 1989. *Investigation of Dielectric Properties of Some Frozen Materials using Cross-borehole Radiowave Pulse Transmission*. US Army Cold Regions Research and Engineering Laboratory, Hanover, New Hampshire. CRREL Report 89–4.

Arcone SA, Chacho EF, Delaney AJ. 1998. Seasonal structure of taliks beneath arctic streams determined with ground-penetrating radar. In *Proceeding of the 7th International Conference on Permafrost*. Centre d'études nordiques, Université Laval: Québec; 19–24.

Asprion U, Aigner T. 1999. Towards realistic aquifer models: three-dimensional georadar surveys of Quaternary gravel deltas (Singen Basin SW Germany). *Sedimentary Geology* **129**: 281–297.

BASC. 2007. Barrow Arctic Science Consortium/Barrow Environmental Observatory. http://www.arcticscience.org/researchBases.php#3 [May 2007].

Beres M, Green A, Huggenberger P, Horstmeyer H. 1995. Mapping the architecture of glaciofluvial sediments with three-dimensional georadar. *Geology* **23**: 1087–1090.

Billings WD, Peterson KM. 1980. Vegetational change and ice-wedge polygons through the thaw-lake cycle in arctic Alaska. *Arctic and Alpine Research* **12**: 413–432.

Bockheim JG, Hinkel KM. 2005. Characteristics and significance of the transition zone in drained thaw-lake basins of the Arctic Coastal Plain, Alaska. *Arctic* **54**: 406–417.

Britton ME. 1966. Vegetation of the arctic tundra. In *Arctic Biology*, Hansen HP (ed.). Oregon State University Press: Corvallis; 26–61.

Brown J. 1967. Tundra soils formed over ice wedges, northern Alaska. *Soil Science Society of America Proceedings* **31**: 686–691.

Brown J. 1969. Soil properties developed on the complex tundra relief of northern Alaska. *Biuletyn Peryglacjalny* **18**: 153–167.

Brown J, Johnson PL. 1965. *Pedo-Ecological Investigations Barrow, Alaska*. US Army Cold Regions Research and Engineering Laboratory, Hanover, New Hampshire. CRREL Technical Report 159: 32 pp.

Brown J, Nelson FE, Hinkel KM. 2000. The Circumpolar Active Layer Monitoring (CALM) program research design and initial results. *Polar Geography* **3**: 165–258.

Carson CE, Hussey KM. 1962. The oriented lakes of arctic Alaska. *Journal of Geology* **70**: 417–439.

Conyers LB, Goodman D. 1997. *Ground-Penetrating Radar: An Introduction for Archaeologists*. Altamir Press: Walnut Creek, California.

Corbeanu RM, McMechan GA, Szerbiak RB, Soegaard K. 2002. Prediction of 3-D fluid permeability and mudstone distributions from ground-penetrating radar (GPR) attributes: Example from the Cretaceous Ferron member, east-central Utah. *Geophysics* **67**: 1495–1504.

Dallimore SR, Davis JL. 1987. Ground-probing radar investigations of massive ground ice and near surface geology in continuous permafrost. In *Current Research, Part A. Geological Survey of Canada, Paper 87–1A*, 913–918.

Doolittle JA, Hardisky MA, Gross MF. 1990. A ground-penetrating radar study of active layer thicknesses in areas of moist sedge and wet sedge tundra near Bethel, Alaska, U.S.A. *Arctic and Alpine Research* **22**: 175–182.

Doolittle JA, Hardisky MA, Black S. 1992. A ground-penetrating radar study of Goodream Palsen, Newfoundland, Canada. *Arctic and Alpine Research* **24**: 173–178.

Eisner WR, Bockheim JG, Hinkel KM, Brown TA, Nelson FE, Peterson KM, Jones BM. 2005. Paleoenvironmental analyses of an organic deposit from an erosional landscape remnant, Arctic Coastal Plain of Alaska. *Palaeogeography, Palaeoclimatology, Palaeoecology* **217**: 187–204.

Estabrook GF, Outcalt S. 1984. An algorithm for clustering profile data and its application to near-surface ice content data from wet coastal tundra soils near Barrow, Alaska. *Mathematical Geology* **16**: 193–205.

French HM. 2007. *The Periglacial Environment*. John Wiley and Sons: Chichester, West Sussex.

Frohn RC, Hinkel KM, Eisner WR. 2005. Satellite remote sensing classification of thaw lakes and drained thaw lake basins on the North Slope of Alaska. *Remote Sensing of Environment* **97**: 116–126.

Grasmueck M, Weger R, Horstmeyer H. 2004. Three-dimensional ground-penetrating radar imaging of sedimentary structures, fractures, and archaeological features at submeter resolution. *Geology* **32**: 933–936.

Green A, Gross R, Holliger K, Horstmeyer H, Baldwin J. 2003. Results of 3-D georadar surveying and trenching the San Andreas Fault near its northern landward limit. *Tectonophysics* **368**: 7–23.

Hinkel KM, Nelson FE. 2003. Spatial and temporal patterns of active layer depths at CALM sites in northern Alaska, 1995–2000. *Journal of Geophysical Research-Atmospheres* **108**(D2): 10.129/2001JD000927.

Hinkel KM, Peterson KM, Eisner WR, Nelson FE, Turner KM, Miller LL, Outcalt SI. 1996. Formation of injection frost mounds over winter 1995–96 at Barrow, Alaska. *Polar Geography* **20**: 235–248.

Hinkel KM, Doolittle JA, Bockheim JG, Nelson FE, Paetzold R, Kimble J, Travis R. 2001. Detection of subsurface permafrost features using ground-penetrating




DOI: 10.1002/ppp

radar, Barrow, Alaska. *Permafrost and Periglacial Processes* **12**: 179–190. DOI: 10.1002/ppp.369.

Hinkel KM, Eisner WR, Bockheim JG, Nelson FE, Peterson KM, Dai XY. 2003. Spatial extent, age, and carbon stock in drained thaw lake basins on the Barrow Peninsula, Alaska. *Arctic, Antarctic, and Alpine Research* **35**: 291–300.

Hinkel KM, Frohn RC, Nelson FE, Eisner WR, Beck RA. 2005. Morphometric and spatial analysis of thaw lakes and drained thaw lake basins in the western Arctic Coastal Plain, Alaska. *Permafrost and Periglacial Processes* **16**: 327–341. DOI: 10.1002/ppp.562.

Hopkins DM. 1949. Thaw lakes and thaw sinks in the Imuruk Lake area, Seward Peninsula. *Journal of Geology* **57**: 119–131.

Horvath CL. 1998. An evaluation of ground-penetrating radar for investigation of palsa evolution, Macmillan Pass, NWT, Canada. In *Proceeding of the 7th International Conference on Permafrost*. Centre d'études nordiques, Université Laval: Québec; 473–478.

Kovacs A, Morey RM. 1985. Impulse radar sounding of frozen ground. In *Workshop on Permafrost Geophysics, Golden, Colorado*. US Army Corps of Engineers, Cold Regions Research and Engineering Laboratory, Hanover, New Hampshire. CRREL Special Report 85–5, 28–40.

Kruse S, Grasmueck M, Weiss M, Viggiano DV. 2006. Sinkhole structure imaging in covered karst terrain. *Geophysical Research Letters* **33**(LI6405): 1–6.

Lehmann F, Green AG. 1999. Semiautomated georadar data acquisition in three dimensions. *Geophysics* **64**(3): 719–731.

Leucci G, Negri S. 2006. Use of ground penetrating radar to map subsurface archaeological features in an urban area. *Journal of Archaeological Science* **33**: 502–512.

MacKay JR. 1983. Downward water movement into frozen ground, western Arctic coast, Canada. *Canadian Journal of Earth Sciences* **20**: 120–134.

Moorman BJ, Robinson SD, Burgess MM. 2003. Imaging periglacial conditions with ground-penetrating radar. *Permafrost and Periglacial Processes* **14**: 319–329. DOI: 10.1002/ppp.463.

Pilon JA, Annan AP, Davis JL. 1985. Monitoring permafrost ground conditions with ground probing radar (G.P.R.). In *Workshop on Permafrost Geophysics, Golden, Colorado*. US Army Corps of Engineers, Cold Regions Research and Engineering Laboratory, Hanover, New Hampshire. CRREL Special Report 85–5, 71–73.

Rand J, Mellor M. 1985. *Ice-coring Augers for Shallow Depth Sampling*. US Army Corps of Engineers, Cold Regions Research and Engineering Laboratory Hanover, New Hampshire. CRREL Report 85–21: 22pp.

Robinson SD, Moorman BJ, Judge AS, Dallimore SR. 1993. The characterization of massive ice at Yaya Lake, Northwest Territories using radar stratigraphy techniques. In *Current Research, Part B. Geological Survey of Canada, Paper 93–1B*; 23–32.

Ross N, Harris C, Christiansen HH, Brabham BJ. 2005. Ground penetrating radar investigations of open system pingos, Adventdalen, Svalbard. *Norwegian Journal of Geography* **59**: 129–138.

Scott WJ, Sellmann P, Hunter JA. 1990. Geophysics in the study of permafrost. In *Geotechnical and Environmental Geophysics, Vol. 1: Review and Tutorial*. Society of Exploration Geophysicists Investigation in Geophysics, No. 5, 355–384.

Seguin MK. 1986. Geophysics of permafrost mounds. *Eos* **67**: 1401.

Sellmann PV, Brown J, Lewellen RI, McKim H, Merry C. 1975. *The Classification and Geomorphic Implications of Thaw Lakes on the Arctic Coastal Plain, Alaska*. US Army Corps of Engineers, Cold Regions Research and Engineering Laboratory, Hanover, New Hampshire. CRREL Special Report 344: 21pp.

Shur Y, Hinkel KM, Nelson FE. 2005. The transient layer: Implications for geocryology and climate-change science. *Permafrost and Periglacial Processes* **16**: 5–17. DOI: 10.1002/ppp.518.

Soil Survey Staff. 2003. *Keys to soil taxonomy* (9th ed.). USDA Natural Resources Conservation Service: Washington, DC.

Sudarmo B, McMechan GA, Epili D. 1996. Simulation and imaging of GPR data scattered by reinforcing bars in concrete bridge deck. *Journal of Environmental and Engineering Geophysics* **1**: 163–170.

Szerbiak RB, McMechan GA, Corbeanu R, Forster C, Snelgrove SH. 2001. 3-D characterization of a clastic reservoir analog: from 3-D GPR data to a 3-D fluid permeability model. *Geophysics* **66**: 1026–1037.

van Dam RL. 2002. Internal structure and development of an aeolian river dune in The Netherlands, using 3-D interpretation of ground-penetrating radar data. *Netherlands Journal of Geosciences* **81**: 27–37.

Wahrhaftig C. 1965. *Physiographic Divisions of Alaska*. USGS Professional Paper 482.

WRCC. 2006. Western Regional Climate Center. http://www.wrcc.dri.edu [May 2007].

Wu T, Shuxun L, Cheng G, Zhuotong N. 2005. Using ground-penetrating radar to detect permafrost degradation in the northern limit of permafrost on the Tibetan Plateau. *Cold Regions Science and Technology* **41**: 211–219.

Yoshikawa K, Leuschen C, Ikeda A, Harada K, Gogineni P, Hoekstra P, Hinzman L, Sawada Y, Matsuoka N. 2006. Comparison of geophysical investigations for detection of massive ground ice (pingo ice). *Journal of Geophysical Research* **111**(E06S19): 1–10. DOI:10.1029/2005JE002573.